Environmental Science & Technology

pubs.acs.org/est

Article

Mechanism of Permselectivity Enhancement in Polyelectrolyte-Dense Nanofiltration Membranes via Surfactant-Assembly Intercalation

Yuanzhe Liang and Shihong Lin*

Cite This: *Environ. Sci. Technol.* 2021, 55, 738–748

Read Online

ACCESS | Metrics & More | Article Recommendations

ABSTRACT: Enhancing the water permeance while maintaining the solute rejection of a nanofiltration (NF) membrane can potentially result in significant cost-reduction for NF—a membrane process that excels in several unique environmental applications of growing interests. In this work, we demonstrate for the first time that intercalation of surfactant self-assemblies in the polyelectrolyte multilayer (PEM) can lead to significant performance enhancement of salt-rejecting dense NF membranes fabricated using layer-by-layer assembly of polyelectrolytes. Specifically, the intercalation of sodium dodecyl sulfate (SDS) bilayers in a PEM comprising poly(diallyldimethylammonium chloride) (PDADMAC) and poly (sodium 4-styrenesulfonate) (PSS) resulted in a decrease in PEM thickness, increase in pore size, and a smoother and more hydrophilic surface. The water permeance of the resulting PEM NF membrane increased by 100% without compromising the rejection of Na_2SO_4. Experiments with a quartz crystal microbalance also provide direct evidence that the intercalation of the surfactants substantially reduces the subsequent adsorption of the polyelectrolytes of a similar charge. Based on its mechanism of performance enhancement, surfactant intercalation may become a universally applicable and highly cost-effective approach for dramatically enhancing the performance of PEM NF membranes.

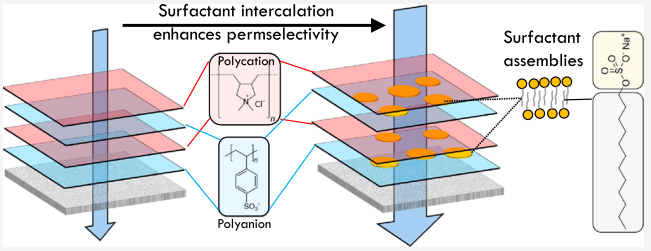

INTRODUCTION

Nanofiltration (NF) has received growing attention in recent years in water and wastewater treatment applications.[1,2] It is an effective and chemical-free membrane process for water softening and has also been widely explored in treating contaminated groundwater and in wastewater reuse.[3−6] The key advantage of NF is the ability to selectively reject the target species while allowing other species to pass through.[7,8] The ability of selective species removal has important practical implications. For example, using NF instead of reverse osmosis (RO) for water softening can potentially save energy due to the lower osmotic pressure difference across an NF membrane leaky to most of the monovalent ions as compared to that across an RO membrane that rejects nearly all ions.[9−11] In another example, NF can be applied in wastewater reuse to remove heavy metals and micropollutants but allow nutrient ions (e.g., phosphate and ammonia) to stay in the permeate for direct fertigation.[12−16] In yet another example, NF can be used to concentrate organic contaminants for more cost-effective chemical treatment (of these contaminants).[17]

NF membranes are generally classified into two major categories based on the pore size.[18] Loose NF (LNF) membranes, which have a typical range of molecular weight cutoff (MWCO) between 500 and 1000 Da and generally low rejections for salts, are often employed to remove dyes and relatively large organic macromolecules such as humic acids. In comparison, tight or dense NF (DNF) membranes, which have an MWCO around 200 Da and near perfect rejection of divalent salts, are typically used for water softening and the removal of heavy metals and emerging organic contaminants. Compared to RO membranes, DNF membranes typically have substantially higher water permeability, which enables the operation at lower pressure and/or higher flux.[19]

In either case, enhancing the cost-effectiveness of NF requires membranes of high permselectivity, i.e., these membranes should have high water permeance and satisfactory rejection of the target species. However, in many cases, there is an intrinsic tradeoff between these two performance metrics, i.e., a membrane with higher water permeance typically has poorer performance in solute rejection.[20,21] Rational and innovative designs of the active layer of NF membranes are

Received: October 12, 2020
Revised: November 24, 2020
Accepted: November 24, 2020
Published: December 8, 2020

required to achieve a high permselectivity.[22−24] Among the different approaches to fabricate NF/RO membranes, using layer-by-layer (LbL) deposition of polyelectrolytes to construct a polyelectrolyte multilayer (PEM) as the active layer for separation is a highly flexible approach with the capability of fine tuning the active layer properties.[25−27]

In fabricating PEM NF membranes using LbL deposition of polyelectrolyte, two types of oppositely charged polyelectrolytes alternately deposit onto an ultrafiltration membrane substrate. The irreversible LbL deposition of polyelectrolytes is mainly driven by electrostatic attractions between the oppositely charged polyelectrolytes.[28−31] With this approach, the LNF membranes are commonly fabricated using at least one weak polyelectrolyte (e.g., one strong and one weak polyelectrolyte or two weak polyelectrolytes),[3,16,32−34] whereas DNF membranes are typically fabricated using two strong polyelectrolytes.[35−38] Several critical membrane properties, such as the pore size distribution, surface charge, and active layer thickness, are affected by multiple factors in the LbL deposition process, such as the type of polyelectrolytes,[39,40] polyelectrolyte concentration,[39] ionic strength of the polyelectrolyte solution,[41−43] pH,[44−46] and temperature.[47,48] Adjusting these parameters provides avenues to control the membrane permeance and ion selectivity. Beyond these parameters, integrating various types of additives (e.g., nanomaterials) into the PEM is also a widely explored approach to enhance the permselectivity.[49,50]

In our recent studies, we reported a novel and cost-effective approach to dramatically enhance the permeance of loose NF membranes for removing macromolecules (e.g., humic acid and dyes).[16,32] This approach is based on the intercalation of surfactant bilayers between weak polycations (polyethylenimine, PEI) and strong polyanions (polystyrene sulfonate, PSS) and has been demonstrated to be capable of enhancing the performance by multiple folds without compromising the rejection of macromolecules. The use of surfactant bilayers as nanometer-thin "structural modifiers" to enhance NF performance is not only conceptually novel and interesting, but also generally more practical as compared to using nanomaterials. However, it remains unclear (1) how surfactant assemblies enhanced the water permeance without compromising solute rejection, and (2) if this novel approach is equally effective for enhancing the performance of salt-rejecting "tight" NF membranes which have an active layer with much smaller pore size than "loose" NF membranes. This work is performed with the aim to address these two questions.

In this study, we investigate how the intercalation of anionic surfactants (sodium dodecylsuflate) between the polycations and polyanions affects the permselectivity of the resulting NF membrane. The dense NF membrane for rejecting Na_2SO_4 is fabricated using two strong polyelectrolytes, poly-(diallyldimethylammonium chloride) as the polycations and poly (sodium 4-styrenesulfonate) as the polyanions. We employ quartz crystal microbalance with dissipation (QCM-D) to investigate the impact of surfactant integration on polyelectrolyte adsorption. We also perform ellipsometry and polarization modulation-infrared reflection adsorption spectroscopy to probe the impact of surfactant integration on the thickness and molecular structure of the resulting PEM films. With PEM NF membranes developed using LbL, we compare the pore size distribution, morphology, and interfacial properties between membranes with and without surfactant intercalation. We also evaluate the impact of surfactant intercalation on the NF performance of the PEM NF membranes and relate the NF performance to the membrane properties. Finally, we evaluate the long-term stability of surfactant-intercalated PEM NF membranes and their stability under various solution and operation conditions.

MATERIALS AND METHODS

Materials and Chemicals. A polyacrylonitrile ultrafiltration (PAN, UF) membrane with a molecular weight cutoff of 50 kDa (GE Healthcare Life Science) was used as the substrate for preparing the polyelectrolyte multilayer NF membrane. Poly (diallyldimethylammoniumchloride) (PDADMAC; MW 400,000−500,000 g mol^{-1}; 20% wt in water), poly (sodium 4-styrenesulfonate) (PSS; MW 1,000,000 g mol^{-1}), sodium dodecyl sulfate (SDS, >99%), sodium dodecylbenzenesulfonate (SDBS, technical grade), (3-aminopropyl) triethoxysilane (APTES) (99%), toluene (anhydrous, 99.8%), hydrochloric acid (HCl, ACS reagent, 37%), sodium hydroxide (NaOH, >98%), Na_2SO_4 (≥99%), $MgSO_4$ (≥99.5%), $MgCl_2$ (≥99.99%), NaCl (≥99%), anhydrous D-(+)-glucose (MW 180 g mol^{-1}, ≥99.5%), sucrose (MW 342 g mol^{-1}, ≥99.5%), and D-(+)-raffinosepentahydrate (MW 594 g mol^{-1}, ≥98%) were purchased from Sigma-Aldrich (St. Louis, MO, USA). All chemicals were used as received without purification. Silicon wafers were purchased from Pure Wafer, Inc. (San Jose, CA, USA). Deionized water (Millipore, USA) was used for solution preparation, membrane cleaning during the LbL process, and NF performance test.

Membrane Fabrication. The PAN substrate membrane was pretreated using 2 M NaOH for 30 min to acquire a negative surface charge and then rinsed with DI water. The reference membranes, namely, $(PD\text{-}PS)_n$ membranes, were prepared via alternate deposition of PDADMAC and PSS with and without the addition of NaCl (concentration varies from 0 to 0.1 M). The hydrolyzed PAN substrate was first exposed to the solution of cationic PDADMAC (1 g L^{-1}) for 30 min, rinsed with DI water for 5 min, then exposed to the solution of anionic PSS (2 g/L^{-1}) for another 30 min, and rinsed with DI water for 5 min. The resulting membrane is referred to as the $(PD\text{-}PS)_1$ with the subscript "1" denoting one PD-PS bilayer. The same deposition cycle was repeated to form additional bilayers (n = 1 to 5). In this study, we focus on making PEM NF for removing salts with divalent anions. Therefore, all membranes fabricated in this study were terminated with a polyanion (PSS) layer. The role of ionic strength on the properties and performance of the $(PD\text{-}PS)_n$ PEM NF membrane was studied by adding NaCl into the aqueous polyelectrolyte solution during LbL deposition.

The fabrication of the SDS-intercalated PEM NF (s-PEM NF) membranes followed a similar procedure as that for preparing the reference PEM NF membranes except for an additional step of surfactant deposition between the polycation and polyanion depositions (Figure 1). Specifically, after each step of PDADMAC deposition, the membrane with the PDADMAC-terminated surface was immersed into an aqueous SDS solution for 30 min (SDS concentration varies from 0 to 1.0 critical micelle concentration, CMC). The SDS-coated PDADMAC surface was rinsed with DI water for 5 min and then further subjected to PSS deposition. The resulting membrane was referred to as the $(PD\text{-}s\text{-}PS)_1$ membrane, with the subscript "1" representing one trilayer of polyelectrolytes and surfactants. The same deposition procedure was repeated to form additional trilayers (n = 1 to 5). When

https://dx.doi.org/10.1021/acs.est.0c06866
Environ. Sci. Technol. 2021, 55, 738−748

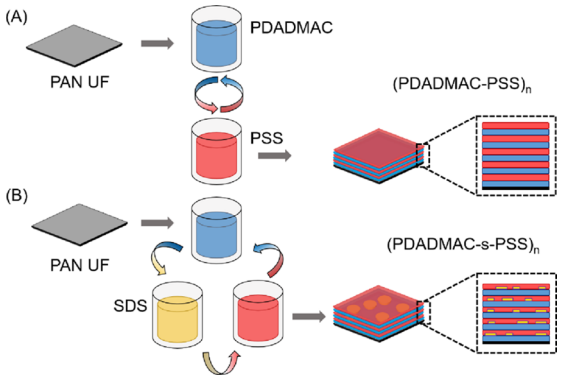

Figure 1. (A) Fabrication of reference $(PD\text{-}PS)_n$ multilayer NF membranes via alternating electrostatic deposition of polycation (PDADMAC) and polyanion (PSS) on a PAN ultrafiltration membrane. (B) Fabrication of the surfactant-integrated $(PD\text{-}s\text{-}PS)_n$ multilayer NF membrane via sequentially electrostatic deposition of polycation (PDADMAC), surfactant (SDS), and polyanion (PSS) on a PAN ultrafiltration membrane.

studying the role of ionic strength on the structure of $(PD\text{-}s\text{-}PS)_n$ PEM NF membranes, NaCl was only added into the polyelectrolyte solutions during membrane fabrication (i.e., it was not added to the surfactant solutions). While the majority of the experimental work focused on using SDS as the intercalating agent, we also followed procedure to fabricate $(PD\text{-}s\text{-}PS)_5$ membranes using SDBS as an alternative intercalating agent to test if it can also enhance PEM NF membrane performance.

Probing Polyelectrolyte Deposition with QCM-D. The adsorption of polyelectrolytes and surfactants was quantified using a QCM-D equipped with a SiO_2-modified quartz crystal sensor (Biolin Scientific Q-Sense E4). The QCM-D system has four parallel flow cells, and a peristaltic pump was used to circulate polyelectrolyte and surfactant solutions through these cells. In a QCM-D measurement, an AC voltage was applied to excite the oscillation of the crystal at its fundamental resonant frequency. The frequency (F) and dissipation (D) was determined by fitting the decay of the crystal oscillation. With QCM-D, we measured the frequency shifts and energy dissipation of the quartz crystal sensor during the polyelectrolyte deposition process, from which we can estimate the temporal evolution of the deposited mass and the viscoelastic properties of each polyelectrolyte layer.

Prior to use, the SiO_2-modified quartz crystal sensor was cleaned with ammonia (25%) and hydrogen peroxide (30%) and rinsed thoroughly with deionized water. The oscillation frequency of the SiO_2-modified quartz crystal sensor was first measured with Milli-Q water at a flow rate of 100 uL min^{-1}. The stable normalized frequency at the third overtone was recorded as the baseline. For the deposition experiments, the aqueous polyelectrolyte solutions (1 g L^{-1} PDADMAC and 2 g L^{-1} PSS) and surfactant solution (SDS at its CMC) were introduced alternately, at a flow rate of 100 uL min^{-1}, following the same deposition sequence as described in the Membrane Fabrication section. Upon adsorption, the resonance frequency of the SiO_2-modified quartz crystal decreases with the continuous increase in the mass of the crystal, which is commonly described by the Sauerbrey relationship:[51,52]

$$\Delta m = -\frac{C\Delta f_n}{n} \quad (1)$$

where Δm is the mass of the polyelectrolyte deposited on the crystal, C is the crystal constant, Δf_n is the shift in resonance frequency, and n is the overtone number (the third overtone is used in this study). Both the frequency and dissipation data were collected at a frequency of 200 Hz. All measurements were carried out at 25 °C.

Measuring PEM Thickness with Ellipsometry. Direct characterization of the film thickness of the PEM on the PAN UF substrate is challenging due to the intrinsic roughness of the porous PAN substrate membrane. Therefore, we constructed the PEM on atomically smooth silicon wafers to characterize the effect of surfactant intercalation on the PEM thickness using ellipsometry. For the thickness measurement, we repeated the LbL assembly of both the $(PD\text{-}PS)_n$ and surfactant-integrated $(PD\text{-}s\text{-}PS)_n$ multilayers (n = 1 to 5) on silicon wafers and measured the thickness of resulting films at different deposition stages using a dual rotating-compensator spectroscopic ellipsometer (J.A. Woollam M-2000VI). The ellipsometer's light source and detector were attached to the chamber at viewport flanges, which were set at ~70° with respect to the sample surface normal. The thickness of each PEM was measured three times at different locations.

Characterizing the Chemical Structure of the PEM Using PM-IRRAS. To explore the effect of surfactant intercalation on the chemical characteristics of the PEM, we investigated the $(PD\text{-}PS)_5$ and $(PD\text{-}s\text{-}PS)_5$ multilayers deposited on Au/Si substrates by polarization modulation-infrared reflection adsorption spectroscopy (PM-IRRAS). PM-IRRAS was performed using a Bruker Tensor 27 Fourier transform infrared spectrometer equipped with a PEM-90 photoelastic modulator and a liquid-nitrogen-cooled mercury cadmium−telluride detector with a nondichroic BaF_2 window. The source beam employed a half-wavelength retardation modulated at a frequency of 50 kHz and the incidence angle is set at 85° to the PEM sample surface. Spectra were collected over 360 scans at a resolution of 4 cm^{-1}.

To prepare a sample for PM-IRRAS characterization, a clean Au/Si substrate was immersed in an ethanol solution of 1 mM thioglycolic acid for 14 h, then washed with an excess amount of ethanol and water, and dried under nitrogen to prepare a negatively charged self-assembled monolayer (SAM) surface. The successful deposition of SAMs was confirmed by the change of the surface wetting property. Specifically, the advancing water contact angle (WCA) changed from 75 ± 3 ° for a pristine Au/Si surface to 5 ± 3° for a SAM/Au/Si surface. The preparation of reference $(PD\text{-}PS)_5$ and SDS-intercalated $(PD\text{-}s\text{-}PS)_5$ PEM films on the SAM surface then followed a similar deposition sequence as mentioned in the Membrane Fabrication section.

Characterizing Membrane Pore Size Distribution and Interfacial Properties. To acquire properties of the PEM that are relevant to separation performance, we measured the surface zeta potentials of the $(PD\text{-}PS)_n$ and $(PD\text{-}s\text{-}PS)_n$ PEM NF membranes at different deposition stages using a streaming potential analyzer (SurPASS electrokinetic analyzer, Anton Paar, Ashland, VA) using an adjustable gap cell with a channel width around 100 um. The zeta potentials of PEM NF membranes at different pH values are determined via a pH titration from 10 to 3 using 1 mM KCl as the electrolyte solution at room temperature.

An optical tensiometer (Theta Lite, Biolin Scientific) was used to measure the contact angle of the $(PD\text{-}PS)_n$ and $(PD\text{-}s\text{-}PS)_n$ PEM NF membranes using the sessile drop method. A

https://dx.doi.org/10.1021/acs.est.0c06866
Environ. Sci. Technol. 2021, 55, 738−748

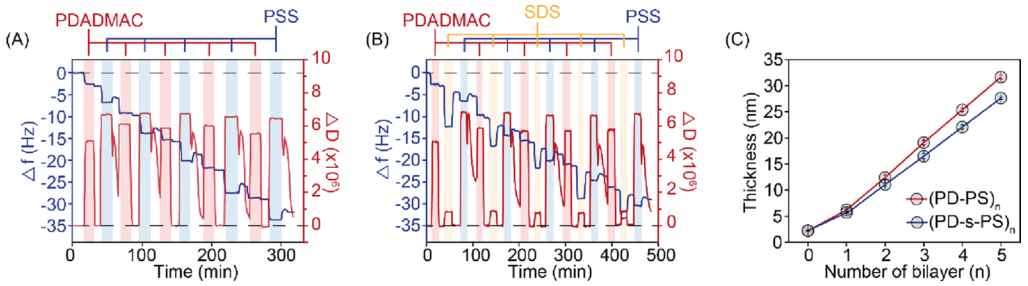

Figure 2. Change of frequency (from the third overtone) and energy dissipation as a function of the adsorption of the first five bilayers of (A) reference $(PD\text{-}PS)_n$ PEM film and (B) surfactant-integrated $(PD\text{-}s\text{-}PS)_n$ PEM film. Red columns represent the deposition step of cationic PDADMAC, blue columns represent the deposition step of anionic PSS, and yellow columns represent the deposition step of SDS. Empty columns between every two-colored columns represent the cleaning steps using DI water. (C) Thickness increment of the reference $(PD\text{-}PS)_n$ and surfactant-integrated $(PD\text{-}s\text{-}PS)_n$ multilayer films on Si wafer as a function of the bilayer number. The reported value represents the average of three measurements and the error bar indicates the standard deviation of three runs.

droplet volume of 5 ± 1 μL of DI water was used for each test at three random locations on three independent PEM NF membranes at different deposition stages. An optical image of the droplet on the surface was taken after being deposited and is used to estimate the contact angle. We also characterized the surface morphology of PEM NF membranes using scanning electron microscopy (SEM, Zeiss Merlin) and atomic force microscopy (AFM, Bruker). The surface roughness of $(PD\text{-}PS)_n$ and $(PD\text{-}s\text{-}PS)_n$ membranes was compared based on the surface topography measured using AFM.

To estimate the pore size distribution of the $(PD\text{-}PS)_n$ and $(PD\text{-}s\text{-}PS)_n$ PEM NF membranes, we tested the PEM NF membranes with a series of neutral organic molecules, including glycerol (92 Da), glucose (180 Da), sucrose (342 Da), raffinose (504 Da), and β-cyclodextrin (1135 Da). The feed concentration of each organic species was 0.2 g L^{-1} and all measurements were carried out with an applied pressure of 4 bar. After the flux became stable, we collected feed and permeate samples and measured their solute concentrations using a Total Organic Carbon (TOC) analyzer. The molecular weight cutoff (MWCO) of the PEM NF membrane is defined as the molecular weight at which the rejection is 90%. The mean pore radius of the PEM NF membrane equals the Stokes radius of the organic solute with a measured rejection of 50%. The distribution of the membrane pore size is determined as the geometric standard deviation of the PDF curve (eq 2), which is the ratio between the Stokes radius corresponding to a rejection of 84.13% and that corresponding to a rejection of 50%.[53]

$$\frac{dR(r_p)}{dr_p} = \frac{1}{r_p \ln \sigma_p \sqrt{2\pi}} \exp\left[-\frac{(\ln r_p - \ln \mu_p)^2}{2(\ln \sigma_p)^2}\right] \quad (2)$$

where μ_p is the mean pore size, σ_p is the geometric standard deviation of the PDF curve, and r_p is the Stokes radius of the organic solute.

Evaluating Membrane Performance in Nanofiltration. We evaluated the water permeance and solute rejection of the $(PD\text{-}PS)_n$ and $(PD\text{-}s\text{-}PS)_n$ PEM NF membranes using a custom-made stainless steel NF cell with crossflow and an effective membrane area of 7.1 cm^2. All measurements were carried out at a constant temperature of 25 ± 0.5 °C and a crossflow velocity of 8.7 cm s^{-1}. Prior to filtration, we compacted the PEM NF membranes overnight at a testing pressure of 4 bar. After compaction, we calculated the pure water permeance (*PWP*, unit: L m^{-2} h^{-1} bar^{-1}) of the PEM NF membrane using the following equation:

$$\mathrm{PWP} = \frac{J_w}{\Delta P} \quad (3)$$

where J_w is the volumetric flux of water (L m^{-2} h^{-1}) and ΔP is the applied pressure (bar), respectively. The salt rejection performance of the $(PD\text{-}PS)_n$ and $(PD\text{-}s\text{-}PS)_n$ PEM NF membranes was evaluated with Na_2SO_4, $MgSO_4$, $MgCl_2$, and NaCl (1 g L^{-1} in all cases). The salt rejection rate was calculated using the following equation.

$$R = \left(1 - \frac{c_p}{c_f}\right) \times 100\% \quad (4)$$

where c_p and c_f are the solute concentration of permeate and feed solution, which are determined by measuring the electrical conductivity of the feed and permeate solution, respectively.

RESULT AND DISCUSSION

Effect of Surfactant Intercalation on the Kinetics of Polyelectrolyte Deposition. The LbL formation of the reference $(PD\text{-}PS)_5$ PEM film and surfactant-integrated $(PD\text{-}s\text{-}PS)_5$ PEM film is quantitatively captured by QCM-D measurements (Figure 2A,B). Based on eq 1, the relationship between adsorbed mass and the shift of resonance frequency from the third overtone, Δf, follows $\Delta m \approx -0.3\Delta f$.

In general, the introduction of polyelectrolyte to a quartz crystal sensor coated with oppositely charged polyelectrolyte led to a sharp decrease in resonance frequency due to the fast adsorption of polyelectrolyte via electrostatic interaction (Figure 2A,B). Comparing the Δf for the adsorption of PDADMAC and PSS reveals that more PSS adsorbed onto the sensor surface than PDADMAC (Figure 2A, blue curve). Flushing the surface with DI water resulted in a negligible change of Δf after PDADMAC adsorption but a significant and consistent increase of Δf after PSS adsorption, likely due to the partial desorption of weakly bound PSS and the swelling of the adsorbed PSS layer.[54] Without intercalation of SDS, the total change of resonant frequency over the deposition of five layers of PD-PS on the SiO_2-coated quartz crystal was ~32 Hz, which corresponds to an areal mass density of 96.1 ± 0.2 ng cm^{-2}.

The adsorption of both PDADMAC and PSS also led to sharp increases of dissipation (Figure 2A, red curve) due to the nonrigid nature of the adsorbed polyelectrolyte layer. However, when rinsing the system with DI water after each

https://dx.doi.org/10.1021/acs.est.0c06866
Environ. Sci. Technol. 2021, 55, 738−748

adsorption step, the dissipation experienced a significant drop because of the reconfiguration of adsorbed polyelectrolyte that resulted in a more compact and rigid layer.[55] In particular, the dissipation always reverted to zero almost immediately when a PDADMAC-coated surface was rinsed with DI water. For PSS-coated surface, however, the decline of dissipation was more gradual and did not reach zero in the limited rinsing time window.

The introduction of SDS dramatically changed the dynamics of the LbL process (Figure 2B). First, we observed from Δf that SDS deposited onto the surface in a substantial amount, resulting in an Δf that is multiple times of that for PDADMAC and PSS adsorption. However, the dissipation induced by SDS adsorption is very small, likely due to the higher degree of rigidness for a layer of short-chain molecules (as compared to polyelectrolytes). Rinsing the SDS-coated surface appeared to remove most of the SDS, suggesting that only part of the adsorbed SDS could remain on the surface after DI water rinsing. (We note that the adsorbed surfactants on a smooth surface form self-assembled bilayers[16,32]). Interestingly, the presence of SDS on the PDADMAC surface reduced the consequent adsorption of PSS. Specifically, the Δf of the first to fifth deposited PSS layers in the absence of SDS was approximately 2.8, 3.1, 3.0, 3.2, and 3.3 Hz, respectively (Figure 2A), much higher than that in the presence of SDS (approximately, 0.9, 1.1, 1.1, 1.1, and 1.1 Hz for the first to fifth layer, Figure 2B).

Because the partial desorption of PSS was as significant in the presence of SDS (Figure 2A) as in the absence of SDS (Figure 2B), the overall effect of less PSS adsorption and similar PSS desorption is the substantially reduced amount of net PSS adsorption in each step. The reduced net PSS adsorption is likely attributable to the presence of adsorbed SDS that occupies part of the positive adsorption sites provided by PDADMAC. The areal mass density of the $(PD\text{-}s\text{-}PS)_5$ membrane was 87.0 ± 0.1 ng cm^{-2}, which is slightly lower than that of the $(PD\text{-}PS)_5$ membrane (96.1 ± 0.2 ng cm^{-2}) even with the additional adsorbed SDS.

Effect of Surfactant Intercalation on the Thickness of the PEM. The impact of SDS intercalation on the thickness of the $(PD\text{-}PS)_n$ PEM film on an atomically smooth silicon wafer was characterized using a spectroscopic ellipsometer and the results are shown in Figure 2C. The thickness increment for the deposition of each bilayer is slightly, but consistently, larger for the reference $(PD\text{-}PS)_n$ multilayer film than for the $(PD\text{-}s\text{-}PS)_n$ multilayer film. In both cases, the thickness increment per additional bi- or trilayer is constant except for the first bi- or trilayer (Figure 2C). Specifically, each additional bi- or trilayer adds 6.1 ± 0.1 nm of thickness increment to the $(PD\text{-}PS)_n$ film and 5.3 ± 0.1 nm to the $(PD\text{-}s\text{-}PS)_n$ film, respectively. The initial nonlinear increment of film thickness was caused by the fact that the first PDADMAC/PSS bilayer may not form a homogenous film and assemble into heterogeneous islands on the silicon wafer.[56−58]

How Does SDS Intercalation Change the PEM Properties? *Chemical Characteristics and Pore Size.* The Fourier transform infrared (FTIR) spectrum of the $(PD\text{-}PS)_5$ PEM film shows two characteristic absorption peaks at 1184 and 1042 cm^{-1} due to the asymmetric and symmetric stretching vibrations of the $-SO^{3-}$ groups from PSS, respectively (Figure 3A). The absorption peak at 1468 cm^{-1} is characteristic of $-CH_3$ bending vibrations in PDADMAC. Notably, no new peak emerges beyond these characteristics of

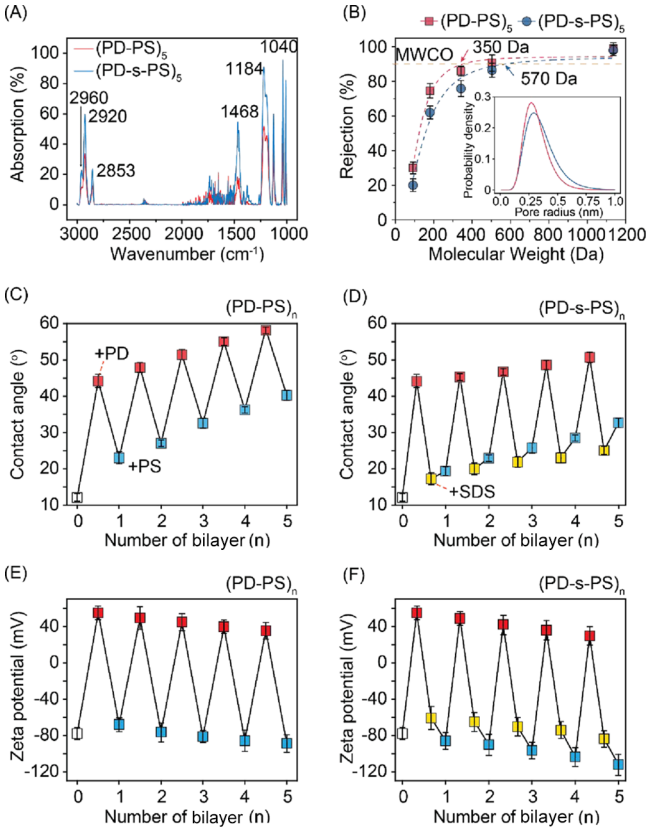

Figure 3. (A) FTIR spectra of the reference $(PD\text{-}PS)_n$ and the surfactant-intercalated $(PD\text{-}s\text{-}PS)_n$ multilayer films on the SAM surface. (B) Impacts of SDS integration on the molecular weight cutoff (MWCO) and pore size distribution of the $(PD\text{-}PS)_5$ and $(PD\text{-}s\text{-}PS)_5$ PEM NF membrane. Contact angle of (C) reference $(PD\text{-}PS)_n$ and (D) surfactant-integrated $(PD\text{-}s\text{-}PS)_n$ PE-NF membranes at different deposition steps. Surface zeta potential of (E) reference $(PD\text{-}PS)_n$ and (F) surfactant-integrated $(PD\text{-}s\text{-}PS)_n$ PE-NF membranes at different deposition steps.

PSS and PDADMAC, which suggests the absence of covalent interaction between the two polyelectrolytes.[59]

The intercalation of SDS into the $(PD\text{-}s\text{-}PS)_5$ PEM was confirmed by the emergence of an absorption peak at 2960 cm^{-1} that corresponds to symmetric $-CH_3$ stretching.[60,61] The presence of SDS increases the intensity of all three characteristic peaks mentioned above due to the reduced crystallinity (increased number of gauche CH_2).[62] The reduction of crystallinity increases the free volume of the PEM and thus potentially affects pore size distribution and enhances membrane permeability. The increase in pore size distribution was confirmed by filtration experiments with a series of neutral organic compounds. Specifically, $(PD\text{-}PS)_5$ and $(PD\text{-}s\text{-}PS)_5$ PEM NF membranes have an MWCO of 350 and 570 Da, respectively (Figure 3B), which correspond to a mean pore size of 0.3 and 0.34 nm, respectively (Figure 3B inset).

Wetting Properties and Surface Potential. The NaOH-treated PAN UF membrane surface became hydrophilic with a WCA of 12° and carried a strongly negative surface charge (Figure 3C−F, white squares). The adsorption of the first layer of PDADMAC increased the WCA to 45° (Figure 3C,D), similar to values reported in the literature.[63,64] It also reversed the surface charge from −78 to 57 mV (Figure 3E). In the absence of SDS, the adsorption of the first layer of PSS substantially reduced the WCA of the surface (Figure 3C) as

https://dx.doi.org/10.1021/acs.est.0c06866
Environ. Sci. Technol. 2021, 55, 738−748

PSS is a more hydrophilic polymer than PDADMAC.[63,64] The adsorption of PSS also reverted the surface potential to be strongly negative (Figure 3E). Repeating the alternate deposition of PDADMAC and PSS always incurred the change in WCA and surface potential in a similar pattern as the first bilayer. However, the WCA of both the PDADMAC-coated surface and PSS-coated surface systematically increased (Figure 3C), while the surface potential of both the PDADMAC-coated surface and PSS-coated surface slightly but systematically decreased (Figure 3E), as the number of bilayers increased.

The adsorption of SDS onto a PDADMAC surface dramatically reduced the WCA (Figure 3D) and surface potential (Figure 3F), which suggests that SDS likely formed a bilayer with one side attaching onto the positively charged PDADMAC surface and the other side exposed. The adsorption of PSS onto an SDS-coated surface only resulted in slight changes of WCA and surface potential because of the suppressed PSS adsorption as shown in the QCM-D results (Figure 2A,B). Notably, the WCA of the $(PD\text{-}s\text{-}PS)_n$ membrane in each deposition step is systematically lower than that of the reference $(PD\text{-}PS)_n$ membrane in the same deposition step (Figure 3C,D), indicating that the SDS intercalation enhances the overall hydrophilicity of the PEM NF membranes. The enhanced hydrophilicity has been reported to be beneficial to membrane permeance.[65,66] Additionally, the SDS intercalation also increases the surface charge/surface potential of the PEM NF membrane, i.e., making the surface more negative (Figure 3E vs Figure 3F), which also contributes to the better rejection of anions due to stronger Donnan exclusion.

Surface Morphology. The integration of SDS to the PEM NF membrane leads to a smoother membrane surface (Figure 4A vs Figure 4B). Visually, the reference $(PD\text{-}PS)_5$ PEM NF membrane has a heterogeneous surface with randomly distributed patches (Figure 4A), whereas the surface of the surfactant-integrated $(PD\text{-}s\text{-}PS)_5$ PEM NF membrane is more homogenous with few patches (Figure 4B). The influence of SDS integration in the surface roughness of the PEM NF membrane is further quantified using AFM (Figure 4C-F). The estimated surface roughness of the reference $(PD\text{-}PS)_5$ membrane and the $(PD\text{-}s\text{-}PS)_5$ membrane is R_q = 37 nm (or R_a = 29 nm) and R_q = 30 nm (or R_a = 21 nm), respectively.

The smoothening of the PEM NF membrane by the intercalation of SDS is likely caused by the dampened adsorption of the similarly charged polyelectrolyte (PSS in this case) onto the SDS-coated surface.[16] For the reference $(PD\text{-}PS)_n$ PEM NF membrane, the PDADMAC-coated surface is of strong positive charge and possesses abundant adsorption sites. Therefore, the PSS adsorption is fast and the density of the adsorbed PSS is high. The chain rearrangement and redistribution of newly adsorbed PSS molecules, which only partially anchor to the substrate and have a high density, are suppressed due to both conformational entropic penalty and steric hindrance from the neighboring PSS polymer chains.[44,46,67]

For a negatively charged SDS-decorated PDADMAC surface (Figure 3F), the electrostatic repulsion between the surface and the PSS polyelectrolytes and the lower density of the available adsorption sites both led to substantially slower adsorption of PSS. Due to the much lower density of available adsorption sites, successful adsorption of PSS may occur only when the orientation of the PSS chains happens to favor the extension of PSS along the surface to maximize the contact between PSS and the available adsorption sites on the SDS-decorated PDADMAC surface. Such a kinetically unfavorable adsorption process shares the similarity with the formation of more "compact" aggregates in reaction-limited aggregation, a well-studied concept in colloidal physics.[68,69] Specifically, the reaction-limited aggregation is a kinetically unfavorable process that allows the primary particles to diffuse deeper into the center of a porous aggregate to form an aggregate of a higher fractal dimension.

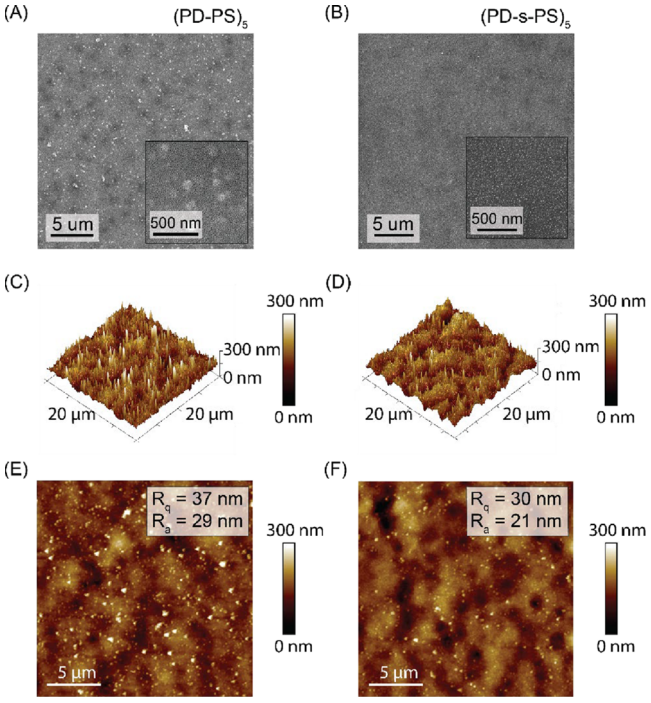

Figure 4. SEM image of (A) reference $(PD\text{-}PS)_5$ and (B) surfactant-integrated $(PD\text{-}s\text{-}PS)_5$ PEM NF membranes. AFM images of (C, E) reference $(PD\text{-}PS)_5$ and (D, F) surfactant-integrated $(PD\text{-}s\text{-}PS)_5$ PEM NF membranes.

Nanofiltration Performance. The intercalation of SDS between the PDADMAC and PSS layers dramatically enhances the permeance of the resulting PEM NF membrane (Figure 5A). The degree of the permeance enhancement is dependent on the number of bi- or trilayers and the ionic strength of the polyelectrolyte solution used for the LbL deposition. The permeance enhancement is the most significant when no NaCl was added in the polyelectrolyte solution, especially for PEM NF membranes with fewer layers. However, we observed that the rejection of Na_2SO_4 was unacceptably low (<90%) when NaCl was not added in the polyelectrolyte solution in the LbL deposition (Figure 5B). This is because the deposition of polyelectrolytes in the presence of salt typically results in the formation of a "denser" polyelectrolyte layer.[38,70,71] Therefore, the following discussion will focus primarily on results obtained with a polyelectrolyte solution containing NaCl.

With both ionic strengths (10 and 100 mM NaCl), the intercalation of SDS nearly doubled the water permeance of the PEM NF membranes (Figure 5A) without compromising the rejection of Na_2SO_4 (Figure 5B). For PEM NF membranes obtained using an ionic strength of 100 mM, the rejections of Na_2SO_4 are 96.5 and 97.6% for the $(PD\text{-}PS)_5$ and $(PD\text{-}s\text{-}PS)_5$ membranes, respectively, whereas the permeance for the two membranes is 5.9 and 11.5 L m^{-2} h^{-1} bar^{-1}, respectively. The

https://dx.doi.org/10.1021/acs.est.0c06866
Environ. Sci. Technol. 2021, 55, 738−748

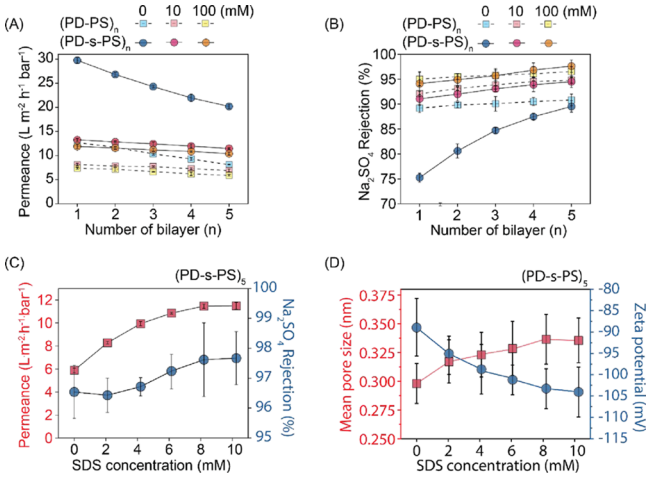

Figure 5. (A) Salt (Na_2SO_4) rejection and (B) membrane permeance of the surfactant-integrated $(PD\text{-}s\text{-}PS)_5$ PEM NF membrane as a function of the bilayer number with varying background ionic strength. (NaCl concentration, mM). The reported value represents the average of three measurements and the error bar indicates the standard deviation of three runs. Impacts of SDS concentration on (C) permselectivity and (D) mean pore size and surface potential of the surfactant-integrated $(PD\text{-}s\text{-}PS)_5$ PEM NF membrane. The reported value represents the average of three measurements and the error bar indicates the standard deviation of three runs.

higher permeance of the $(PD\text{-}s\text{-}PS)_5$ membrane is attributable to its larger pore size distribution as compared to the reference $(PD\text{-}PS)_5$ membrane (Figure 3B), which in turn is caused by less adsorption of PSS with SDS intercalation (Figure 2A,B) that also results in a thinner membrane (Figure 2C).

Despite the doubling of water permeance, the rejection of Na_2SO_4 was not compromised (Figure 5B). This is partly because the integration of SDS also renders the $(PD\text{-}s\text{-}PS)_5$ membrane slightly more negatively charged than the $(PD\text{-}PS)_5$ membrane (Figure 3E,F). In other words, the weakened steric exclusion due to a larger pore distribution in a $(PD\text{-}s\text{-}PS)_5$ membrane is partially compensated by the stronger Donnan exclusion due to a stronger negative membrane charge. However, it does not require "stronger repulsion" of the solute to maintain or even enhance rejection when water permeance increases substantially, which can be illustrated using the definition of solute rejection as shown in equation 5:

$$R = \left(1 - \frac{J_s}{J_w c_f}\right) \times 100\% \quad (5)$$

where J_s is the solute flux. While J_s tends to increase with increasing J_w that enhances advective solute transport, as long as J_s does not increase as rapidly as J_w, a higher R can be achieved mostly due to the substantial improvement of J_w.

The impacts of SDS concentration on the membrane permeance and Na_2SO_4 rejection of the $(PD\text{-}s\text{-}PS)_n$ membrane (fabricated using polyelectrolyte solutions with an ionic strength of 100 mM) is summarized in Figure 5C. Both the permeance and Na_2SO_4 rejection increases with increasing SDS concentration. Based on the explanation that SDS intercalation enhances permselectivity by enlarging pores and the increasing surface charge (Figure 5D), a higher SDS concentration is expected to result in more SDS adsorption and thus larger improvement of permselectivity. Interestingly, the impacts of SDS concentration on permeance and Na_2SO_4 rejection appear to taper off and reach a limit around the critical micelle concentration (~8.2 mM), which suggests that the adsorption of SDS on the PDADMAC surface reaches a maximum when the SDS concentration reaches the critical micelle concentration. This is likely because only free surfactants (i.e., those not being part of a micelle) can effectively adsorb onto the PDADMAC surface to form SDS bilayers, which is consistent with the observation in a previous study for surfactant adsorption onto particulate surfaces.[72]

The performance of the surfactant-intercalated $(PD\text{-}s\text{-}PS)_n$ PEM NF membrane was further evaluated using other types of salts, including $MgSO_4$, $MgCl_2$, and NaCl, with the results compared with the reference $(PD\text{-}PS)_5$ membrane (Figure 6).

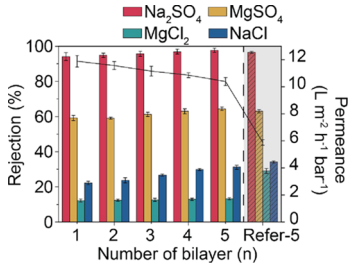

Figure 6. Permselectivity comparison of the reference $(PD\text{-}PS)_5$ and $(PD\text{-}s\text{-}PS)_n$ PEM NF membranes with a different number of bilayers. The reported value represents the average of three measurements and the error bar indicates the standard deviation of three runs.

For the $(PD\text{-}s\text{-}PS)_n$ membrane, the rejection of all four salts increases slightly with an increasing number of bilayers, but at the cost of a moderate reduction in membrane permeance. Compared to the reference $(PD\text{-}PS)_5$ membrane, the $(PD\text{-}s\text{-}PS)_5$ membrane has similar or even better rejection of the sulfate salts, i.e., Na_2SO_4 and $MgSO_4$, but a lower rejection of NaCl and $MgCl_2$, in particular $MgCl_2$. The similarity and difference between the two membranes in rejecting different types of ions can be readily explained by the Donnan exclusion mechanism. As both membranes are negatively charged, they are effective in rejecting salts with divalent anions. For the same reason, neither membrane is effective in rejecting salts with divalent cations and monovalent anions, such as $MgCl_2$. However, because the $(PD\text{-}s\text{-}PS)_5$ membrane is more negatively charged than the $(PD\text{-}PS)_n$ membrane, the rejection of $MgCl_2$ by the $(PD\text{-}s\text{-}PS)_5$ membrane is lower than that by the $(PD\text{-}PS)_5$ membrane. For the rejection of NaCl, Donann exclusion plays a less important role. Therefore, both membranes have a low rejection of NaCl but the $(PD\text{-}PS)_5$ membrane has a slightly higher rejection due to its smaller pore size distribution. If the treatment objective for the membrane is to remove sulfate, the ideal membrane in the investigated series appears to be the $(PD\text{-}s\text{-}PS)_1$ membrane with one bilayer intercalated with SDS, considering both water permeance and salt rejection performance.

Based on the mechanism discussed above, the intercalation of anionic surfactant (SDS) in the performance enhancement of the $(PD\text{-}s\text{-}PS)_n$ PEM NF membrane primarily has two major roles: (1) it reduces the amount of PSS adsorption, making a more compact and thinner PEM NF membrane; (2) it slightly enlarges the pore size but at the same time enhances the membrane surface charge. Simply reducing the amount of PSS adsorption by decreasing the PDADMAC concentration in fabricating the reference $(PD\text{-}PS)_5$ membrane (without adding

https://dx.doi.org/10.1021/acs.est.0c06866
Environ. Sci. Technol. 2021, 55, 738−748

surfactants) can reduce the thickness of the PEM NF membrane and achieve a dramatic increase in water permeance (Table 1). However, the Na_2SO_4 rejection of the resulting

Table 1. Permeance, Na_2SO_4 Rejection, Zeta Potential, Mean Pore Size, and Thickness of the $(PD\text{-}PS)_5$ PEM NF Membrane and SDS-Intercalated and SDBS-Intercalated $(PD\text{-}s\text{-}PS)_5$ PEM NF Membranes[a]

	$(PD\text{-}PS)_5$ reference[b]	$(PD\text{-}PS)_5$ (PD 0.5 g/L)	$(PD\text{-}s\text{-}PS)_5$ (SDS 1 CMC)[e]	$(PD\text{-}s\text{-}PS)_5$ (SDBS 1 CMC)[f]
thickness[c] (nm)	31.7 ± 0.2	20.4 ± 0.2	27.1 ± 0.3	29.6 ± 0.3
Na_2SO_4 Rejection (%)	96.5 ± 3.2	54.6 ± 2.9	97.7 ± 3.8	97.5 ± 4.5
permeance (L m^{-2} h^{-1} bar^{-1})	5.9 ± 0.4	16.3 ± 1.1	11.5 ± 0.6	9.4 ± 0.4
zeta potential[d] (mV)	-88.9 ± 6.7	-68.4 ± 5.3	-103.2 ± 5.9	-94.2 ± 7.5
mean Pore size (nm)	0.30 ± 0.02	0.31 ± 0.02	0.34 ± 0.02	0.32 ± 0.02

[a]Each data is obtained based on three replicate experiments and the error represents standard deviation. [b]All PEM NF membranes are fabricated using PD (1 g/L) and PS (2 g/L) unless specified otherwise. [c]Thickness is measured using ellipsometry by depositing PEM on a silicon wafer. [d]Testing pH of zeta potential is 7.06 ± 0.14. [e]SDS concentration is 8.2 mM. [f]SDBS concentration is 0.4 mM.

membrane becomes heavily compromised due to the substantially lower (negative) surface charge (Table 1). Therefore, intercalation of surfactant assemblies represents a more accurate tuning method that preserves the salt rejection performance of the resulting membrane. Lastly, we also show that intercalation of another surfactant, SDBS, which has similar characteristics to SDS, can also result in similar but slightly inferior performance enhancement as that achieved by SDS intercalation(Table 1). We believe SDBS is not as effective as SDS because SDBS has a lower packing density (or surface excess) due to the presence of a bulkier benzene ring.[73]

Stability of the Surfactant-Intercalated PEM NF Membrane. The performance of the PEM NF membrane was mostly stable under different operation and solution conditions and over long-term operation (Figure 7). Specifically, while the fluxes of both the $(PD\text{-}s\text{-}PS)_5$ and reference $(PD\text{-}PS)_5$ membranes increased roughly linearly at higher pressure, the Na_2SO_4 rejections by both membranes were barely compromised (Figure 7A). When both membranes were subjected to feed solutions of a wide range of pH, we observed that Na_2SO_4 rejections decreased with decreasing pH but only became considerably compromised when the pH was very low (Figure 7B). The dependence of Na_2SO_4 rejection on pH is consistent with the dependence of the surface charge of the PSS-coated PEM surface (Figure 7C). Interestingly, the SDS-intercalated $(PD\text{-}s\text{-}PS)_5$ PEM NF membrane still maintained a Na_2SO_4 rejection of ~90% at a pH of 3 when the Na_2SO_4 rejection of the $(PD\text{-}PS)_5$ PEM NF membrane had declined to 70%. The improved Na_2SO_4 rejection of the SDS-intercalated $(PD\text{-}s\text{-}PS)_5$ PEM NF membrane is caused by both the substantial increase in membrane permeance and the substantially less positive charge of the membrane at pH = 3. Specifically, the reference $(PD\text{-}PS)_5$ membrane at pH = 3 has a zeta potential of 17.6 mV and thus promoted the transport of SO_4^{2-} better than the SDS-intercalated $(PD\text{-}s\text{-}PS)_5$ membrane

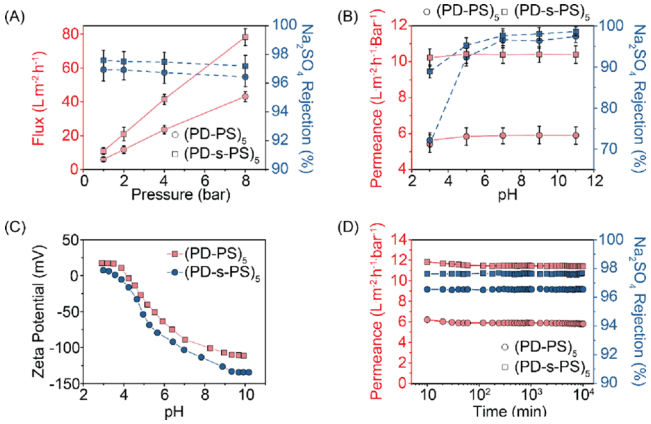

Figure 7. Stability evaluation of $(PD\text{-}PS)_5$ PEM NF and surfactant-intercalated $(PD\text{-}s\text{-}PS)_5$ PEM NF membranes (A) under various applied pressure and (B) at various testing pH. (Na_2SO_4 concentration: 1000 ppm and pressure for pH stability evaluation: 4 bar). The reported value represents the average of three measurements and the error bar indicates the standard deviation of three runs. (C) pH-dependent surface zeta potentials of $(PD\text{-}PS)_5$ and $(PD\text{-}s\text{-}PS)_5$ PEM NF membranes. (D) Long-term stability test of $(PD\text{-}PS)_5$ PEM NF and surfactant-intercalated $(PD\text{-}s\text{-}PS)_5$ PEM NF membranes. (Na_2SO_4 concentration: 1000 ppm, pressure: 4 bar, and time span: 7 days).

which has a zeta potential of 6.8 mV. We can therefore conclude that the intercalation of SDS improves the stability of the PEM NF membranes under acidic conditions. While these experiments with different pH values were only performed for 12 h, a recent study has reported that $(PD\text{-}PS)_n$ PEM NF membranes can maintain stable performance in extreme pH in a filtration experiment spanning over two months.[74] Lastly, we also performed NF experiments for one week with both $(PD\text{-}PS)_5$ and $(PD\text{-}s\text{-}PS)_5$ membranes and found that their performance in terms of both water permeance and Na_2SO_4 rejection were stable throughout the experiments(Figure 7D), which also suggests that relative performance advantage of the $(PD\text{-}s\text{-}PS)_5$ membrane vs reference $(PD\text{-}PS)_5$ was also maintained in long-term NF operation.

IMPLICATIONS

We have demonstrated in this study that the intercalation of SDS bilayers in PEM-based dense NF membranes can double the permeance without compromising salt rejection. Using multiple characterization techniques and by performing experiments on both model PEM films and PEM NF membranes, we find that the reduced adsorption of the polyelectrolyte, enlarged pore structure, and enhanced surface hydrophilicity are likely the major causes of the substantially enhanced water permeance. The intercalation of the surfactant (bilayers) represents an emerging strategy, an alternative to the widely used method of embedding nanoparticles, to tailor and improve the performance of NF membranes. While such a method of surfactant intercalation has been proven successful for loose NF membranes that reject organic macromolecules, this study demonstrates its applicability for salt-rejecting dense NF membranes that have far more stringent requirements on the integrity and properties of the separation layer. These results suggest the possible universal effectiveness of this method of intercalation of surfactant-bilayers on all PEM NF membranes fabricated using LbL deposition of polyelectrolytes, which leads to vast opportunities of substantially

https://dx.doi.org/10.1021/acs.est.0c06866
Environ. Sci. Technol. 2021, 55, 738−748

enhancing the performance of the many PEM NF membranes that have been and will be developed.

AUTHOR INFORMATION

Corresponding Author

Shihong Lin − *Department of Civil and Environmental Engineering, Interdisciplinary Material Science Program, and Department of Chemical and Biomolecular Engineering, Vanderbilt University, Nashville, Tennessee 37235, United States*; orcid.org/0000-0001-9832-9127; Email: shihong.lin@vanderbilt.edu

Author

Yuanzhe Liang − *Department of Civil and Environmental Engineering and Interdisciplinary Material Science Program, Vanderbilt University, Nashville, Tennessee 37235, United States*

Complete contact information is available at: https://pubs.acs.org/10.1021/acs.est.0c06866

Notes

The authors declare no competing financial interest.

ACKNOWLEDGMENTS

The authors are thankful for the support from the Desalination and Water Purification Research Program of the US Bureau of Reclamation via agreement R18AC00110 and from the US-Israel Binational Agricultural and Development Fund (BARD) (award no. IS-5209-19).

REFERENCES

(1) Mohammad, A. W.; Teow, Y. H.; Ang, W. L.; Chung, Y. T.; Oatley-Radcliffe, D. L.; Hilal, N. Nanofiltration Membranes Review: Recent Advances and Future Prospects. *Desalination* **2015**, *356*, 226−254.

(2) Ng, L. Y.; Mohammad, A. W.; Ng, C. Y. A Review on Nanofiltration Membrane Fabrication and Modification Using Polyelectrolytes: Effective Ways to Develop Membrane Selective Barriers and Rejection Capability. *Adv. Colloid Interface Sci.* **2013**, *197-198*, 85−107.

(3) Boo, C.; Wang, Y.; Zucker, I.; Choo, Y.; Osuji, C. O.; Elimelech, M. High Performance Nanofiltration Membrane for Effective Removal of Perfluoroalkyl Substances at High Water Recovery. *Environ. Sci. Technol.* **2018**, *52*, 7279−7288.

(4) Washington, J. W.; Jenkins, T. M.; Rankin, K.; Naile, J. E. Decades-Scale Degradation of Commercial, Side-Chain, Fluorotelomer-Based Polymers in Soils and Water. *Environ. Sci. Technol.* **2015**, *49*, 915−923.

(5) Choo, K. H.; Kwon, D. J.; Lee, K. W.; Choi, S. J. Selective Removal of Cobalt Species Using Nanofiltration Membranes. *Environ. Sci. Technol.* **2002**, *36*, 1330−1336.

(6) Luo, J.; Ding, L.; Wan, Y.; Paullier, P.; Jaffrin, M. Y. Application of NF-RDM (Nanofiltration Rotating Disk Membrane) Module under Extreme Hydraulic Conditions for the Treatment of Dairy Wastewater. *Chem. Eng. J.* **2010**, *163*, 307−316.

(7) Epsztein, R.; Shaulsky, E.; Dizge, N.; Warsinger, D. M.; Elimelech, M. Role of Ionic Charge Density in Donnan Exclusion of Monovalent Anions by Nanofiltration. *Environ. Sci. Technol.* **2018**, *52*, 4108−4116.

(8) Liang, Y.; Zhu, Y.; Liu, C.; Lee, K. R.; Hung, W. S.; Wang, Z.; Li, Y.; Elimelech, M.; Jin, J.; Lin, S. Polyamide Nanofiltration Membrane with Highly Uniform Sub-Nanometre Pores for Sub-1 Å Precision Separation. *Nat. Commun.* **2020**, *11*, 2015.

(9) Lin, S. Energy Efficiency of Desalination: Fundamental Insights from Intuitive Interpretation. *Environ. Sci. Technol.* **2020**, *54*, 76−84.

(10) Semiat, R. Energy Issues in Desalination Processes. *Environ. Sci. Technol.* **2008**, *42*, 8193−8201.

(11) Elimelech, M.; Phillip, W. A. The Future of Seawater Desalination: Energy, Technology, and the Environment. *Science* **2011**, *333*, 712−717.

(12) Nghiem, L. D.; Schäfer, A. I.; Elimelech, M. Pharmaceutical Retention Mechanisms by Nanofiltration Membranes. *Environ. Sci. Technol.* **2005**, *39*, 7698−7705.

(13) Zhu, W. P.; Sun, S. P.; Gao, J.; Fu, F. J.; Chung, T. S. Dual-Layer Polybenzimidazole/Polyethersulfone (PBI/PES) Nanofiltration (NF) Hollow Fiber Membranes for Heavy Metals Removal from Wastewater. *J. Memb. Sci.* **2014**, *456*, 117−127.

(14) Hong, S. U.; Ouyang, L.; Bruening, M. L. Recovery of Phosphate Using Multilayer Polyelectrolyte Nanofiltration Membranes. *J. Memb. Sci.* **2009**, *327*, 2−5.

(15) Ali, N.; Halim, N. S. A.; Jusoh, A.; Endut, A. The Formation and Characterisation of an Asymmetric Nanofiltration Membrane for Ammonia-Nitrogen Removal: Effect of Shear Rate. *Bioresour. Technol.* **2010**, *101*, 1459−1465.

(16) Liang, Y.; Lin, S. Intercalation of Zwitterionic Surfactants Dramatically Enhances the Performance of Low-Pressure Nanofiltration Membrane. *J. Memb. Sci.* **2020**, *596*, 117726.

(17) Pica, N. E.; Funkhouser, J.; Yin, Y.; Zhang, Z.; Ceres, D. M.; Tong, T.; Blotevogel, J. Electrochemical Oxidation of Hexafluoropropylene Oxide Dimer Acid (Gen X): Mechanistic Insights and Efficient Treatment Train with Nanofiltration. *Environ. Sci. Technol.* **2019**, *53*, 12602−12609.

(18) Hoek, E. M. V.; Tarabara, V. V. *Encyclopedia of Membrane Science and Technology*; Wiley Online Library, 2013; Vol. 3. DOI: 10.1002/9781118522318.

(19) Petersen, R. J. Composite Reverse Osmosis and Nanofiltration Membranes. *J Membrane Sci* **1993**, *83*, 81−150.

(20) Park, H. B.; Sagle, A. C.; McGrath, J. E.; Freeman, B. D. Water Permeability and Water/Salt Selectivity Tradeoff in Polymers for Desalination. *AIChE Annu. Meet. Conf. Proc.* **2008**, *369*, 130−138.

(21) Park, H. B.; Kamcev, J.; Robeson, L. M.; Elimelech, M.; Freeman, B. D. Maximizing the Right Stuff: The Trade-off between Membrane Permeability and Selectivity. *Science* **2017**, *356*, 1138−1148.

(22) Werber, J. R.; Osuji, C. O.; Elimelech, M. Materials for Next-Generation Desalination and Water Purification Membranes. *Nat. Rev. Mater.* **2016**, *1*, 16018.

(23) Werber, J. R.; Deshmukh, A.; Elimelech, M. The Critical Need for Increased Selectivity, Not Increased Water Permeability, for Desalination Membranes. *Environ. Sci. Technol. Lett.* **2016**, *3*, 112−120.

(24) Teng, X.; Fang, W.; Liang, Y.; Lin, S.; Lin, H.; Liu, S.; Wang, Z.; Zhu, Y.; Jin, J. High-Performance Polyamide Nanofiltration Membrane with Arch-Bridge Structure on a Highly Hydrated Cellulose Nanofiber Support. *Sci. China Mater.* **2020**. DOI: 10.1007/s40843-020-1335-x.

(25) Richardson, J. J.; Björnmalm, M.; Caruso, F. Technology-Driven Layer-by-Layer Assembly of Nanofilms. *Science* **2015**, *348*, No. aaa2491.

(26) Richardson, J. J.; Cui, J.; Björnmalm, M.; Braunger, J. A.; Ejima, H.; Caruso, F. Innovation in Layer-by-Layer Assembly. *Chem. Rev.* **2016**, *116*, 14828−14867.

(27) Shan, W.; Bacchin, P.; Aimar, P.; Bruening, M. L.; Tarabara, V. V. Polyelectrolyte Multilayer Films as Backflushable Nanofiltration Membranes with Tunable Hydrophilicity and Surface Charge. *J. Memb. Sci.* **2010**, *349*, 268−278.

(28) Borges, J.; Mano, J. F. Molecular Interactions Driving the Layer-by-Layer Assembly of Multilayers. *Chem. Rev.* **2014**, *114*, 8883−8942.

(29) Ariga, K.; Hill, J. P.; Ji, Q. Layer-by-Layer Assembly as a Versatile Bottom-up Nanofabrication Technique for Exploratory Research and Realistic Application. *Phys. Chem. Chem. Phys.* **2007**, *9*, 2319−2340.

(30) Bertrand, P.; Jonas, A.; Laschewsky, A.; Legras, R. Ultrathin Polymer Coatings by Complexation of Polyelectrolytes at Interfaces: Suitable Materials, Structure and Properties. *Macromol. Rapid Commun.* **2000**, *21*, 319−348.
(31) Penfold, N. J. W.; Parnell, A. J.; Molina, M.; Verstraete, P.; Smets, J.; Armes, S. P. Layer-By-Layer Self-Assembly of Polyelectrolytic Block Copolymer Worms on a Planar Substrate. *Langmuir* **2017**, *33*, 14425−14436.
(32) Shan, L.; Liang, Y.; Prozorovska, L.; Jennings, G. K.; Ji, S.; Lin, S. Multifold Enhancement of Loose Nanofiltration Membrane Performance by Intercalation of Surfactant Assemblies. *Environ. Sci. Technol. Lett.* **2018**, *5*, 668−674.
(33) Lin, J.; Ye, W.; Zeng, H.; Yang, H.; Shen, J.; Darvishmanesh, S.; Luis, P.; Sotto, A.; Van der Bruggen, B. Fractionation of Direct Dyes and Salts in Aqueous Solution Using Loose Nanofiltration Membranes. *J. Memb. Sci.* **2015**, *477*, 183−193.
(34) Han, G.; Chung, T. S.; Weber, M.; Maletzko, C. Low-Pressure Nanofiltration Hollow Fiber Membranes for Effective Fractionation of Dyes and Inorganic Salts in Textile Wastewater. *Environ. Sci. Technol.* **2018**, *52*, 3676−3684.
(35) Cheng, W.; Liu, C.; Tong, T.; Epsztein, R.; Sun, M.; Verduzco, R.; Ma, J.; Elimelech, M. Selective Removal of Divalent Cations by Polyelectrolyte Multilayer Nanofiltration Membrane: Role of Polyelectrolyte Charge, Ion Size, and Ionic Strength. *J. Memb. Sci.* **2018**, *559*, 98−106.
(36) Ouyang, L.; Malaisamy, R.; Bruening, M. L. Multilayer Polyelectrolyte Films as Nanofiltration Membranes for Separating Monovalent and Divalent Cations. *J. Memb. Sci.* **2008**, *310*, 76−84.
(37) Hong, S. U.; Malaisamy, R.; Bruening, M. L. Separation of Fluoride from Other Monovalent Anions Using Multilayer Polyelectrolyte Nanofiltration Membranes. *Langmuir* **2007**, *23*, 1716−1722.
(38) DuChanois, R. M.; Epsztein, R.; Trivedi, J. A.; Elimelech, M. Controlling Pore Structure of Polyelectrolyte Multilayer Nanofiltration Membranes by Tuning Polyelectrolyte-Salt Interactions. *J. Memb. Sci.* **2019**, *581*, 413−420.
(39) Kujawa, P.; Moraille, P.; Sanchez, J.; Badia, A.; Winnik, F. M. Effect of Molecular Weight on the Exponential Growth and Morphology of Hyaluronan/Chitosan Multilayers: A Surface Plasmon Resonance Spectroscopy and Atomic Force Microscopy Investigation. *J. Am. Chem. Soc.* **2005**, *127*, 9224−9234.
(40) Deng, H. Y.; Xu, Y. Y.; Zhu, B. K.; Wei, X. Z.; Liu, F.; Cui, Z. Y. Polyelectrolyte Membranes Prepared by Dynamic Self-Assembly of Poly (4-Styrenesulfonic Acid-Co-Maleic Acid) Sodium Salt (PSSMA) for Nanofiltration (I). *J. Memb. Sci.* **2008**, *323*, 125−133.
(41) Dubas, S. T.; Schlenoff, J. B. Factors Controlling the Growth of Polyelectrolyte Multilayers. *Macromolecules* **1999**, *32*, 8153−8160.
(42) Klitzing, R. V. Internal Structure of Polyelectrolyte Multilayer Assemblies. *Phys. Chem. Chem. Phys.* **2006**, *8*, 5012−5033.
(43) Lösche, M.; Schmitt, J.; Decher, G.; Bouwman, W. G.; Kjaer, K. Detailed Structure of Molecularly Thin Polyelectrolyte Multilayer Films on Solid Substrates as Revealed by Neutron Reflectometry. *Macromolecules* **1998**, *31*, 8893−8906.
(44) Choi, J.; Rubner, M. F. Influence of the Degree of Ionization on Weak Polyelectrolyte Multilayer Assembly. *Macromolecules* **2005**, *38*, 116−124.
(45) Schönhoff, M.; Bieker, P. Linear and Exponential Growth Regimes of Multilayers of Weak Polyelectrolytes in Dependence on PH. *Macromolecules* **2010**, *43*, 5052−5059.
(46) Shiratori, S. S.; Rubner, M. F. PH-Dependent Thickness Behavior of Sequentially Adsorbed Layers of Weak Polyelectrolytes. *Macromolecules* **2000**, *33*, 4213−4219.
(47) Salomäki, M.; Vinokurov, I. A.; Kankare, J. Effect of Temperature on the Buildup of Polyelectrolyte Multilayers. *Langmuir* **2005**, *21*, 11232−11240.
(48) Tan, H. L.; McMurdo, M. J.; Pan, G.; Van Patten, P. G. Temperature Dependence of Polyelectrolyte Multilayer Assembly. *Langmuir* **2003**, *19*, 9311−9314.
(49) Liu, Y.; Zheng, S.; Gu, P.; Ng, A. J.; Wang, M.; Wei, Y.; Urban, J. J.; Mi, B. Graphene-Polyelectrolyte Multilayer Membranes with Tunable Structure and Internal Charge. *Carbon* **2020**, *160*, 219−227.
(50) Wang, M.; Wang, Z.; Wang, X.; Wang, S.; Ding, W.; Gao, C. Layer-by-Layer Assembly of Aquaporin z-Incorporated Biomimetic Membranes for Water Purification. *Environ. Sci. Technol.* **2015**, *49*, 3761−3768.
(51) Gutierrez, L.; Aubry, C.; Cornejo, M.; Croue, J. P. Citrate-Coated Silver Nanoparticles Interactions with Effluent Organic Matter: Influence of Capping Agent and Solution Conditions. *Langmuir* **2015**, *31*, 8865−8872.
(52) Chen, K. L.; Elimelech, M. Aggregation and Deposition Kinetics of Fullerene (C60) Nanoparticles. *Langmuir* **2006**, *22*, 10994−11001.
(53) Chen, G. E.; Liu, Y. J.; Xu, Z. L.; Tang, Y. J.; Huang, H. H.; Sun, L. Fabrication and Characterization of a Novel Nanofiltration Membrane by the Interfacial Polymerization of 1, 4-Diaminocyclohexane (DCH) and Trimesoyl Chloride (TMC). *RSC Adv.* **2015**, *5*, 40742−40752.
(54) Guzmán, E.; Ritacco, H.; Ortega, F.; Svitova, T.; Radke, C. J.; Rubio, R. G. Adsorption Kinetics and Mechanical Properties of Ultrathin Polyelectrolyte Multilayers: Liquid-Supported versus Solid-Supported Films. *J. Phys. Chem. B* **2009**, *113*, 7128−7137.
(55) Notley, S. M.; Eriksson, M.; Wågberg, L. Visco-Elastic and Adhesive Properties of Adsorbed Polyelectrolyte Multilayers Determined in Situ with QCM-D and AFM Measurements. *J. Colloid Interface Sci.* **2005**, *292*, 29−37.
(56) Iturri Ramos, J. J.; Stahl, S.; Richter, R. P.; Moya, S. E. Water Content and Buildup of Poly (Diallyldimethylammonium Chloride)/Poly (Sodium 4-Styrenesulfonate) and Poly(Allylamine Hydrochloride)/Poly(Sodium 4-Styrenesulfonate) Polyelectrolyte Multilayers Studied by an in Situ Combination of a Quartz Crystal Microb. *Macromolecules* **2010**, *43*, 9063−9070.
(57) Porcel, C.; Lavalle, P.; Ball, V.; Decher, G.; Senger, B.; Voegel, J. C.; Schaaf, P. From Exponential to Linear Growth in Polyelectrolyte Multilayers. *Langmuir* **2006**, *22*, 4376−4383.
(58) McAloney, R. A.; Sinyor, M.; Dudnik, V.; Cynthia Goh, M. Atomic Force Microscopy Studies of Salt Effects on Polyelectrolyte Multilayer Film Morphology. *Langmuir* **2001**, *17*, 6655−6663.
(59) Bhalerao, U. M.; Acharya, J.; Halve, A. K.; Kaushik, M. P. Controlled Drug Delivery of Antileishmanial Chalcones from Layer-by-Layer (LbL) Self Assembled PSS/PDADMAC Thin Films. *RSC Adv.* **2014**, *4*, 4970−4977.
(60) Viana, R. B.; Da Silva, A. B. F.; Pimentel, A. S. Infrared Spectroscopy of Anionic, Cationic, and Zwitterionic Surfactants. *Adv. Phys. Chem.* **2012**, *2012*, 1.
(61) Sperline, R. P. Infrared Spectroscopic Study of the Crystalline Phases of Sodium Dodecyl Sulfate. *Langmuir* **1997**, *13*, 3715−3726.
(62) Prosser, A. J.; Franses, E. I. Infrared Reflection Absorption Spectroscopy (IRRAS) of Aqueous Nonsurfactant Salts, Ionic Surfactants, and Mixed Ionic Surfactants. *Langmuir* **2002**, *18*, 9234−9242.
(63) SU, B.; Wang, T.; Wang, Z.; Gao, X.; Gao, C. Preparation and Performance of Dynamic Layer-by-Layer PDADMAC/PSS Nanofiltration Membrane. *J. Memb. Sci.* **2012**, *423-424*, 324−331.
(64) Elzbieciak, M.; Kolasinska, M.; Warszynski, P. Characteristics of Polyelectrolyte Multilayers: The Effect of Polyion Charge on Thickness and Wetting Properties. *Colloids Surfaces A* **2008**, *321*, 258−261.
(65) Yan, F.; Chen, H.; Lü, Y.; Lü, Z.; Yu, S.; Liu, M.; Gao, C. Improving the Water Permeability and Antifouling Property of Thin-Film Composite Polyamide Nanofiltration Membrane by Modifying the Active Layer with Triethanolamine. *J. Memb. Sci.* **2016**, *513*, 108−116.
(66) Chen, Q.; Yu, P.; Huang, W.; Yu, S.; Liu, M.; Gao, C. High-Flux Composite Hollow Fiber Nanofiltration Membranes Fabricated through Layer-by-Layer Deposition of Oppositely Charged Cross-linked Polyelectrolytes for Dye Removal. *J. Memb. Sci.* **2015**, *492*, 312−321.

https://dx.doi.org/10.1021/acs.est.0c06866
Environ. Sci. Technol. 2021, 55, 738−748

(67) Park, S. Y.; Rubner, M. F.; Mayes, A. M. Free Energy Model for Layer-by-Layer Processing of Polyelectrolyte Multilayer Films. *Langmuir* **2002**, *18*, 9600−9604.
(68) Lin, M. Y.; Lindsay, H. M.; Weitz, D. A.; Ball, R. C.; Klein, R.; Meakin, P. Universality in Colloid Aggregation. *Nature* **1989**, *339*, 360−362.
(69) Weitz, D. A.; Huang, J. S.; Lin, M. Y.; Sung, J. Limits of the Fractal Dimension for Irreversible Kinetic Aggregation of Gold Colloids. *Phys. Rev. Lett.* **1985**, *54*, 1416−1419.
(70) Schoeler, B.; Kumaraswamy, G.; Caruso, F. Investigation of the Influence of Polyelectrolyte Charge Density on the Growth of Multilayer Thin Films Prepared by the Layer-by-Layer Technique. *Macromolecules* **2002**, *35*, 889−897.
(71) Schönhoff, M. Layered Polyelectrolyte Complexes: Physics of Formation and Molecular Properties. *J. Phys. Condens. Matter* **2003**, *15*, R1781.
(72) Carswell, A. D. W.; Lowe, A. M.; Wei, X.; Grady, B. P. CMC Determination in the Presence of Surfactant-Adsorbing Inorganic Particulates. *Colloids Surfaces A Physicochem. Eng. Asp.* **2003**, *212*, 147−153.
(73) Banipal, T. S.; Kaur, H.; Banipal, P. K.; Sood, A. K. Effect of Head Groups, Temperature, and Polymer Concentration on Surfactant-Polymer Interactions. *J. Surfact Deterg.* **2014**, *17*, 1181−1191.
(74) Elshof, M. G.; de Vos, W. M.; de Grooth, J.; Benes, N. E. On the Long-Term PH Stability of Polyelectrolyte Multilayer Nanofiltration Membranes. *J. Memb. Sci.* **2020**, *615*, 118532.

https://dx.doi.org/10.1021/acs.est.0c06866
Environ. Sci. Technol. 2021, 55, 738−748